Submitted to the International Europhysics Conference on High–Energy Physics, HEP99
Tampere, Finland, July 99

Study of the photon remnant in resolved processes at HERA

H1 Collaboration

Abstract

Events with a resolved photon, $x_\gamma < 0.75$, and two hard jets in the final state are used to study the transverse momentum of the photon remnant in photo – and low – Q^2 ($1.4 \leq Q^2 \leq 25$ GeV^2) production. The average transverse momentum of the photon remnant in the $\gamma^* p$ system is found to increase weakly with the virtuality Q^2 of the photon and with the scale of the hard subprocess. The results are satisfactorily simulated by the Monte Carlo program HERWIG.

1 Introduction

In lepton-lepton and lepton-hadron collisions [1, 2], the incoming leptons can act as sources of virtual photons, which are subsequently probed in hard collisions with partons from the other beam particle. Previous studies concerned the region of very small photon virtualities Q^2, where the scattered electron goes close to the beam line, i.e. photoproduction processes with typically $\langle Q^2 \rangle \leq 1$ GeV^2. The transition between photoproduction and deep – inelastic scattering with typically $1 \leq Q^2 \leq 50$ GeV^2 was also studied in [3],[4] and [5].

As the photon virtuality increases, the photon has less and less time to develop those aspects of its hadronic structure that depend on large distances and its interactions may therefore be easier calculable by perturbative means. Hard scattering between an almost real photon and proton is expected, in lowest order of QCD, to occur by two different mechanisms. The photon may interact directly with a quark or gluon from the proton or it may fluctuate into quarks and gluons which then interact with the partons from the proton. These two processes are called direct and resolved, respectively. In the kinematic region where $Q^2 \ll 4P_T^2$ (with $2P_T$ as the hard scale for the production of jets with transverse momentum P_T), the underlying mechanism of jet production is basically the same as for the real photon and the corresponding cross–sections are thus also given as sums of direct and resolved contributions. It must, however, be kept in mind that this intuitively clear distinction between direct and resolved contributions holds only in leading order.

In resolved processes only a fraction of the momentum of the photon is involved in the hard collision, while the remaining momentum is carried by spectator partons. These partons fragment into a photon remnant jet which is expected to be approximately collinear with the original photon. Therefore in most Monte Carlo simulations the resolved photon is modeled as a hadron with collinear incoming partons.

So far two methods have been proposed to study the properties of the photon remnant. One is to treat it as an energy deposit close to the direction of the photon [6]. An alternative one is to use jet algorithms which are able to find low p_t remnant jets [7],[8].

The photon remnant was studied by the ZEUS collaboration in photoproduction events [9] using the k_t clustering algorithm. Its properties were found to be consistent with those commonly attributed to jets. The mean transverse momentum of the photon remnant with respect to the beam axis, was measured to be 2.1 ± 0.2 GeV. The fraction of the incident photon's energy, which is reconstructed in the photon remnant jet, was analyzed by H1 in the region $0 \leq Q^2 \leq 49$ GeV^2 in [3]. The evolution of this fraction with Q^2 was found to be consistent with the picture of a resolved photon contribution which is suppressed with increasing virtuality.

In this paper, the properties of photon remnant jet are studied for photoproduction events and for events with low Q^2. The dependence of the p_t of the photon remnant jet on the virtuality Q^2 and the scale of an accompanying hard process are compared with Monte Carlo predictions. The data were collected by the H1 detector in 1995.

2 Detector description

A detailed description of the H1 detector can be found elsewhere [10] and only the components relevant for this analysis are described here.

The coordinate system used has the nominal interaction point as the origin and the incident proton beam defining the $+z$ direction. A finely grained Liquid Argon Calorimeter [11] covers the range in polar angle $4° < \theta < 154°$, with full azimuthal acceptance. It consists of an electromagnetic section with lead absorbers, 20-30 radiation length in depth, and a hadronic section with steel absorbers. The total depths of the calorimeter ranges from 4.5 to 8 hadronic interaction lengths. The energy resolution is $\sigma(E)/E \approx 0.5/\sqrt{E} \oplus 0.02$ for charged pions (E in GeV), as measured in test beams [12]. The hadronic energy measurement is performed by applying a weighting technique in order to account for the non–compensating nature of the calorimeter. The absolute hadronic energy scale is presently known to 4%.

A series of interleaved drift and multiwire proportional chambers surround the interaction region, enabling the reconstruction of charged particles in the range $5° < \theta < 165°$, and the determination of the event vertex. A uniform axial magnetic field of 1.15 T is provided by a superconducting coil which surrounds the calorimeter.

The polar region $153° < \theta < 177.8°$ is covered by the SPACAL [13], a lead/scintillating–fibre calorimeter with both, electromagnetic and hadronic sections. The energy resolution for the electromagnetic section has been determined as $7.5\%/\sqrt{E(\mathrm{GeV})} \oplus 2.5\%$ and the energy scale uncertainty is 2%. The hadronic energy scale uncertainty is presently about 7% [14],[15]. Both calorimeter sections have a time resolution better than 1 ns, enabling the reduction of proton induced background. The SPACAL was used both to trigger on and measure the scattered positron in DIS processes for $0.35 < Q^2 < 100$ GeV^2. In front of the SPACAL, in the direction to the interaction vertex, an eight layer drift chamber BDC [16] covers the polar angle of 151° to 177.5°. It improves the positron identification with the SPACAL and together with the event vertex determination from the central and forward trackers, it gives a precision measurement of the positron scattering angle of 1 mrad.

The luminosity system consists of two crystal calorimeters with resolution $\sigma(E)/E \approx 0.1/\sqrt{E}$ (E in GeV). The electron tagger is located at $z = -33$ m and the photon detector at $z = -103$ m. The electron tagger accepts electrons (positrons) with energy between 0.25 and 0.7 of the incident beam energy and with scattering angles $\theta' < 5$ mrad ($\theta' = \pi - \theta$)

3 Data Samples and Event Selection

The analysis is based on data taken in 1995 with the H1 detector operating at the lepton-proton collider HERA, with positrons of 27.5 GeV colliding with protons of 820 GeV. The integrated luminosity used for this analysis is 1.05 pb^{-1}.

The events were selected according to the kinematic properties determined by measurements of the scattered positron and the hadronic final state. The following variables are used:

$$Q^2 = 4E_eE_e^{'}\sin^2(\theta^{'}/2), \qquad y = 1 - E_e^{'}/E_e\cos^2(\theta^{'}/2), \tag{1}$$

calculated from the positron beam energy E_e, the energy $E_e^{'}$ and the polar angle $\theta^{'}$ of the scattered positron.

In this analysis two data samples were used:

1. **$\mathbf{1.4 < Q^2 < 25}$ GeV^2**: For this low Q^2 sample with jets a set of triggers was used which require the presence of a local energy deposit (cluster) in the SPACAL with energy greater than about 5 GeV in coincidence with an ep bunch crossing. The efficiency of this trigger set is above 97 % over the whole kinematic range. Furthermore the events have to satisfy the following criteria:

   - the most energetic cluster in the electromagnetic section of the SPACAL is a positron candidate (detailed selection criteria described in [17]) with a signal within a time window of 10 ns total width around the expected value for genuine ep collisions;

- $\sum(E_h - p_{z,h}) = E - p_z > 35$ GeV, where E_h and $p_{z,h}$ are the energy and longitudinal momentum of a particle. The sum is over all energy deposits measured with the calorimeters improved by additional tracking information as explained below.

2. $\mathbf{Q^2 < 10^{-2}}$ $\mathbf{GeV^2}$: The photoproduction sample in which the scattered positron is detected in the electron tagger of the luminosity system. The events were triggered by demanding an energy deposit in the electron tagger with $E_{etag} > 4$ GeV in coincidence with at least one track pointing to the vertex region ($p_T > 500$ MeV). In order to suppress random coincidences between the high rate of bremsstrahlung events, ep $\to$ epγ, and p-gas background in the main H1 detector, events were rejected, if a photon with an energy $E_\gamma > 2$ GeV was detected in the photon tagger. This cut also reduces QED radiative corrections to the ep Born cross section.

In addition, for both data samples, the z$-$ coordinate of the interaction vertex was required to be within 35 cm of the nominal position. The variable y was restricted to $0.25 < y < 0.7$ and $0.3 < y < 0.7$ for low Q^2 and photoproduction samples respectively [1] .

An efficient reduction of the background from non-ep interactions was provided by the lower y-cut and the vertex requirements for both data samples. Monte Carlo (MC) studies have shown that the background from photoproduction events to the low Q^2 sample in which the scattered positron escapes the main detector along the beam pipe and the positron signal is faked by an energy deposition associated with the hadronic final state is reduced significantly by the requirements on $E - p_z$ and the presence of two jets. The residual background was found to be less than 1% of the total sample.

To compensate for losses in the calorimetric measurement of hadrons, tracks reconstructed in the central drift chamber were used in addition to calorimetric clusters. The momentum vector of a calorimetric cluster was calculated from its energy deposit in the calorimeter and its direction, which was obtained using the interaction vertex and the cluster center of gravity. Each reconstructed central track with momentum p_{ch} was used with the momentum p_{lim}=min(p_{ch}, p_{const}). The direction of p_{lim} coincides with the direction of p_{ch}. The value of p_{const} was determined by the requirement of a balance between $p_{t,e'}$, the transverse momentum of the scattered positron, and $p_{t,h}$, the transverse momentum of the observed hadrons, and by the requirement that the difference in $E - p_z$ for initial and final states is close to zero. For data we obtained the value p_{const}= 400 MeV.

4 Photon remnant jet identification

It was shown [8] that the jet algorithm DECO is able not only to reconstruct jets from the hard process but also the photon remnant. In DECO jets are made by splitting the event into a sequence of subsets of particles, with the number of subsets running from 2 up to 5 ("jet multiplicity"). The decomposition into subsets (multiplets) is achieved by minimizing a jet function evaluated from the whole event. The jet function used here was thrust, extended up to 5 directions. DECO allows to reconstruct jets with any p_t and any mass.

In the process of jet finding with DECO we proceeded in the following way: since the photon remnant is defined as the remains of the incoming photon, we employ the trick of first adding the γ^* four–vector as an initiator vector for the photon remnant jet, which improves the resolution significantly. The proton four-vector is added as initiator for the proton spectator jet. Initiators are also used in other jet algorithms, for example by the k_t algorithm. Then DECO decomposes

[1]This difference in the range of y gives only about 4% different mean values of the total hadronic energy $< W >$ for both samples.

every event into 4 jets in the laboratory system. It should be noted that DECO is fully Lorentz invariant [8]. The jet with the largest p_z component (relatively to the proton direction) is, as MC studies have shown, the proton spectator jet and is excluded from further analysis. Then we transform the jets from the laboratory to the γ^*p system. The jet with the smallest p_z component in the γ^*p system is assumed to be the candidate for photon remnant jet. Next we subtract the auxiliary virtual photon four–vector from the four–vector of the photon remnant jet candidate. When there was no other object in the photon remnant jet except for this auxiliary four–vector, then there is no photon remnant jet and the event is a direct photon candidate (note that in this limiting case $x_\gamma = 1$). If the photon remnant jet contains objects, the event is accepted as a candidate for the resolved photon process. The two other jets are then assumed to be jets from the hard process. These assumptions about the hard jets and the photon remnant jet are supported by MC studies shown later.

Events are now selected in which the two hard jets satisfy the conditions:

$$p_T^{(i)} \geq 5 \text{ GeV}, \quad -3 \leq \eta^{(\mathrm{i})} \leq 0, \quad |\mathrm{p_T^{(1)}} + \mathrm{p_T^{(2)}} > 12 \text{ GeV}, \tag{2}$$

where the transverse momenta $p_T^{(i)}$ and pseudorapidities $\eta^{(i)}$ are calculated in the γ^*p system with the positive z–axis along the incident proton direction. An additional cut was applied to the difference in angles of the jets in the azimuthal plane, $|\varphi^{(1)} - \varphi^{(2)}| \geq 2$ rad. MC studies have shown that this cut [2] reduces the background from jets which could not be assigned to a corresponding jet at the parton level of the leading order QCD MC including parton showers.

It was shown [18] that the backward energy (corresponding to the existence of a photon remnant jet) is strongly correlated with x_γ. The variable x_γ allows us to separate direct and resolved component with a reasonable accuracy. In our investigations we determined it using

$$x_\gamma = \frac{\sum\limits_{i=1}^{2} (E_i - p_{z,i})}{\sum\limits_{h=1}^{N} (E_h - p_{z,h})}, \tag{3}$$

where the sum runs over the two jets in the numerator and over all hadrons in the event in the denominator.

MC studies indicate that the $x_\gamma < 0.75$ region is dominated by the resolved component, with a small tail of direct component (for HERWIG MC $\sim 3\%$ of cross section for photoproduction, $\sim$17% for low Q^2 sample, depending on Q^2). Therefore, to enrich our data sample with resolved photon events the cut $x_\gamma < 0.75$ was applied.

In total 5387 photoproduction and 1156 low Q^2 events satisfied all cuts.

5 Models

We used two Monte Carlo programs for the modeling of photoproduction and low Q^2 data.

HERWIG [19] is a general purpose MC event generator, applicable to a wide range of hard processes in collisions of many different beam particles. It has a sophisticated treatment of parton showers, based on the idea of color coherence, and a simple model to simulate soft processes accompanying a hard scattering process. Hadronization is done via decay of colorless clusters, formed during the hard scattering and parton shower stages.

[2] It reduces the data samples for photoproduction and low Q^2 by 7% and 5%, respectively.

RAPGAP [20], formulated originally for the simulation of diffractive processes, has recently been extended to several other processes in ep collisions, including jet production. It combines standard hard scattering matrix element and parton showers with LUND string fragmentation using JETSET [21]. As an option, it offers the color dipole model [22] as an alternative model for parton cascading.

In this paper we used HERWIG and RAPGAP for the simulation of the direct as well as the resolved photon components. In the direct channel both HERWIG and RAPGAP generate events according to the exact matrix elements of the 2→3 subprocesses

$$\mathrm{e}+\mathrm{q} \rightarrow \mathrm{e}+\mathrm{q}+\mathrm{g}, \tag{4}$$
$$\mathrm{e}+\mathrm{g} \rightarrow \mathrm{e}+\mathrm{q}+\overline{\mathrm{q}}. \tag{5}$$

In the resolved photon channel both generators use the Equivalent Photon Approximation (EPA) with exact kinematics at the electron vertex but include only the transverse component of the virtual photon inside the beam electron.

In its standard version HERWIG employs the NLO formula for $\alpha_s(\mu)$. We have modified HERWIG to use the LO form of $\alpha_s(\mu)$ which is also the default in RAPGAP and which gives a better description of our data [23].

For the photon parton density functions (PDF) of the virtual photon we use the GRV LO parameterizations for the real photon combined with the simple Drees–Godbole virtuality suppression factor [24]

$$L(Q^2, M^2, \omega^2) \equiv \frac{\ln((M^2+\omega^2)/(Q^2+\omega^2))}{\ln((M^2+\omega^2)/\omega^2)}, \tag{6}$$

where M is the hard scale and ω a free parameter which should be fitted to data. The PDFs of the virtual photon are obtained from those of the real photon by multiplying the latter by L in the case of quarks and by L^2 in the case of gluons.

The distribution of the intrinsic momentum p_t of the partons in the photon and the proton (at the beginning of the initial parton showers) was taken as Gaussian

$$\mathrm{dN}/\mathrm{dp_t^2} \propto \exp(-\mathrm{p_t^2}/\mathrm{k_0^2}) \tag{7}$$

with $k_0 = 0.66$ GeV in both HERWIG and RAPGAP.

It is well known that the properties of jets with moderate p_T are significantly influenced by additional soft particles accompanying the basic parton level hard scattering but not originating from it. It is therefore important that the Monte Carlo used describes correctly the transverse energy flow also outside the jets. In HERWIG these soft particles are optionally generated via the mechanism called *soft underlying event* (SUE). The basic result of this mechanism is a redistribution of energy and momentum of particles coming from the decay of the resolved photon and proton remnant beam clusters. In HERWIG without the SUE, these remnant clusters have typically large relative momenta and, consequently, their decay particles are separated by a large gap in rapidity. Most of these particles remain inside the beam pipe and therefore do not influence the jet properties. The essence of the SUE is to allow these beam clusters to "collide" in a manner typical for soft hadronic (eg. pp) collisions, thereby producing many soft particles occupying the central region between the original beam remnant clusters, where the hard jets are usually located. In events with a SUE the jet characteristics of low p_T jets may be significantly distorted by the accompanying soft particles. The fraction of events in which the hard scattering is accompanied by a SUE is given by the parameter PRSOF in HERWIG 5.9. We recall that there is no such additional mechanism in RAPGAP.

6 Corrections to acceptance and resolution

Events generated with the HERWIG MC were passed through a detailed simulation of the H1 detector and were used to correct for detector resolution and acceptance.

The parameter $p_T^{\rm min}$ in HERWIG and RAPGAP specifies the minimal transverse momentum of the basic parton level hard scattering process in the γ^*p system; we took $p_T^{\rm min} = 3$ GeV for the low Q^2 and $p_T^{\rm min} = 2.5$ GeV for the photoproduction sample. The parameter regulating the amount of the soft underlying event activity in HERWIG was determined from the study of the transverse energy flow outside the jets and from jet profiles to be PRSOF$= 0.1 - 0.2$ [23]. We used 0.2 (0.15) for the photoproduction (low Q^2) sample, respectively.

The value $\omega = 0.2$ GeV (used in eq. (6)) was found to give a reasonable description of dijet cross sections with HERWIG and RAPGAP [5].

HERWIG has been used to study the effects of the detector smearing. In Figure 1 the correlation between the x_γ as reconstructed in the detector and the x_γ as determined from the hadonic final state is shown: good correlation is observed in this variable as well as in $p_T^{(1)} + p_T^{(2)}$. The correlation for $\mathrm{p_t}$, azimuthal angle φ and the pseudorapidity η of the photon remnant jet is also satisfactory, as seen in Figure 2. Because of the good correlation between detector and hadron level distributions and the satisfactory description of the data by MC (not shown here), HERWIG can be used to correct the measured photon remnant distributions for acceptance and resolution effects of the detector.

The $\mathrm{p_t}$ distribution of the photon remnant jet was corrected using an unfolding procedure [25] based on Bayes theorem. The iterative procedure requires a 2-dimensional correlation function between the observable measured with the detector (F^{det}) and the observable reconstructed from the hadronic final state (F^{had}), which was obtained using HERWIG.

Resolved photon events were defined by requiring $x_\gamma < 0.75$. However, as MC studies have shown, in this region of x_γ we still have a tail of direct events – at the level of a few percent, depending on Q^2. The uncertainty of the determination of this background was included in the systematic error and is less than 7% for both data samples.

The following sources of systematic errors have been taken into account (the effect on $< p_t >$ is indicated in brackets):

- A 4% (7%) scale uncertainty of the hadronic energy in the LAr (SPACAL)($< 5\%(< 2\%)$).
- Unfolding procedure uncertainty ($< 10\%$).
- A 1.4% uncertainty in the luminosity determination (negligible)
- The center of bin correction ($< 5\%$).
- The uncertainty connected with the subtraction of direct processes ($< 7\%$).
- Trigger inefficiences ($< 4\%$).

In the low Q^2 sample these additional sources of systematic errors have been taken into account:

- The influence of the measurement errors of the positron on the Lorentz transformation and to the momenta of the jets ($< 1\%$)
- The uncertainty of the positron energy scale in the SPACAL, varying from 0.7% at $E_e' = 27.5$ GeV to 2.5% at $E_e' = 7$ GeV [14] ($< 2\%$).
- Effects of QED radiation ($< 8\%$).

7 Results

In Figure 3 the corrected differential cross sections $\mathrm{d}\sigma/\mathrm{dp_t}$ of the photon remnant jet are presented for different intervals of photon virtuality Q^2 for data and HERWIG. In Figure 4 the corrected mean $\mathrm{p_t}$ values for data and HERWIG are shown as a function of Q^2. A fit to $a + bQ^2$ gives a=1.79$\pm$0.08 and b=0.03$\pm$0.02, which is compatible with a weak increase with Q^2. HERWIG qualitatively describes the observed Q^2 dependence. The $< p_t >$ of the photon remnant jet of HERWIG at the parton level, as also displayed in Fig. 4, shows a similar rise with Q^2, albeit at a lower value. It suggests that the hadronization in HERWIG increases $< p_t >$ but does not change much the shape of the parton level dependence. We can compare our photoproduction value of $< p_t >= 1.85 \pm 0.10$ GeV with the ZEUS result of $< p_t >= 2.1 \pm 0.2$ GeV. Within errors the results are the same. The ZEUS experiment has used the k_T jet algorithm and a sample of events with hard jets with $p_T^{(i)} > 6$ GeV and $\eta_i < 1.6$, in the laboratory frame [9].

The corrected differential cross sections $\mathrm{d}\sigma/\mathrm{dp_t}$ of the photon remnant jet are shown for four different intervals of the hard scale, $p_T^{(1)} + p_T^{(2)}$, in Figure 5 and Figure 6 for photoproduction and the low Q^2 sample, respectively, together with the HERWIG predictions. In Figure 7 the corrected mean p_t values for both data samples are compared with results from HERWIG and RAPGAP. We can conclude that the $< p_t >$ is rising with increasing $p_T^{(1)} + p_T^{(2)}$ for data. Moreover, the dependence seems to be the same within errors for the photoproduction and low Q^2 samples. In order to check that the rise in mean $\mathrm{p_t}$ with the hard scale of the jets is not caused by energy from the hard jets leaking into the proton remnant jet, events were discarded for which the distance $R = \sqrt{\Delta\varphi^2 + \Delta\eta^2}$ between the remnant jet and each one of the two hard jets was less than 2. The remaining events displayed a similar clear rise as the full sample.

HERWIG shows a similar dependence on the hard scale, however, it predicts smaller values of $< p_t >$ for photoproduction and larger ones for the low Q^2 sample. RAPGAP, using the same intrinsic $\mathrm{p_t}$ distribution (eq. (7)) with the same parameter $k_0 = 0.66$ GeV as used in HERWIG, gives too small mean values of $\mathrm{p_t}$ and no dependence on the scale $p_T^{(1)} + p_T^{(2)}$.
It was checked that the rise of $< p_t >$ with $p_T^{(1)} + p_T^{(2)}$ in HERWIG is not due to the presence of the soft underlying event activity . Furthermore the mean value of p_t was found to depend very weakly on the value of the parameter k_0 in HERWIG. The most important process which was found to be responsible for the magnitude of the mean $< p_t >$ and its dependence on the hard scale is the presence of initial parton showers.

8 Conclusions

The $\mathrm{d}\sigma/\mathrm{dp_t}$ distributions and the mean p_t of the photon remnant jet have been studied with the H1 detector for both photoproduction and low Q^2 data. They have been measured as a function of the photon virtuality Q^2 and the scale $p_T^{(1)} + p_T^{(2)}$ of the two hard jets in the event, and they have been compared to the HERWIG MC model. In general HERWIG gives a more satisfactory description of the data than RAPGAP.

The mean $\mathrm{p_t}$ of the photon remnant jet is found to be compatible with a weak increase with Q^2 as might be expected from a photon shrinking with Q^2.

A clear increase of the mean $\mathrm{p_t}$ is found for increasing scale $p_T^{(1)} + p_T^{(2)}$ of the hard subprocess. This dependence is found to be the same, within errors, for both photoproduction and low Q^2 data.

References

[1] PLUTO Collaboration, Ch. Berger et al., Phys. Lett. **B142** (1984) 111;
PLUTO Collaboration, Ch. Berger et al., Phys. Lett. **B281** (1987) 365;
PLUTO Collaboration, Ch. Berger et al., Phys. Lett. **B107** (1981) 168;
JADE Collaboration, W. Bartel et al., Z. Phys. **C24** (1984) 231;
TASSO Collaboration, M. Althoff et al., Z. Phys. **C31** (1986) 527;
TPC/2γ Collaboration, H. Aihara et al., Phys. Rev. Lett. **58** (1987) 97;
TPC/2γ Collaboration, H. Aihara et al., Z. Phys. **C34** (1987) 1;
CELLO Collaboration, H.-J. Behrend et al., contributed to the XXVth Int. Con. on HEP, Singapore 1990, unpublished;
AMY Collaboration, T. Sasaki et al., Phys. Lett. **B252** (1990) 491;
AMY Collaboration, B. J. Kim et al., Phys. Lett. **B325** (1994) 248;
TOPAZ Collaboration, H. Hayashii et al., Phys. Lett. **B314** (1993) 149.

[2] OPAL Collaboration, R. Ackers et al., Z. Phys. **C61** (1994) 199;
ALEPH Collaboration, D. Buskulic et al., Phys. Lett. **B313** (1993) 509;
DELPHI Collaboration, P. Abreu et al., Phys. Lett bf B342 (1995) 402;
ZEUS Collaboration, M. Derrick et al., Phys. Lett. **B322** (1994) 287;
H1 Collaboration, T. Ahmed et al., Nucl. Phys. **B445** (1995) 195;
H1 Collaboration, S. Aid et al., Z. Phys. **C70** (1996) 17;
ZEUS Collaboration, M. Derrick et al., Phys. Lett. **B348** (1995) 665;
ZEUS Collaboration, M. Derrick et al., Phys. Lett **B384** (1996) 401;
ZEUS Collaboration, J. Breitweg et al., Eur. Phys. J. **C1** (1998) 109;
H1 Collaboration, C. Adloff et al., Eur. Phys. J. **C1** (1998) 97.

[3] H1 Collaboration, C. Adloff et al., Phys. Lett. **B415** (1997) 418.

[4] M. Taševský, Proceedings of the International Workshop DIS 98, Brussels, April 1998.

[5] H1 Collaboration, *Measurement of Dijet Cross-Sections at Low Q^2 and the Extraction of an Effective Parton Density of the Virtual Photon*, DESY-98-205, 1998.

[6] G. D'Agostini,G. Monaldi, Proceedings of the Workshop "Physics at HERA", Hamburg 1991,p. 527.

[7] A. Valkarova, Proceedings of the Workshop "Physics at HERA", Hamburg 1991,p. 535.

[8] A.Valkárová, G. Knies, Comparison of Cone and Event-Decomposition Algorithms in Resolved Photon Reactions, DESY 94-047 (1994).

[9] ZEUS Collaboration, M. Derrick et al.,Phys. Lett. **B354** (1995) 163.

[10] H1 Collaboration, I. Abt et al., Nucl. Instr. and Meth. **A386** (1997) 310 and **A386** (1997) 348.

[11] H1 Calorimeter Group, B. Andrieu et al., Nucl. Instr. and Meth. **A336** (1993) 460.

[12] H1 Calorimeter Group, B. Andrieu et al., Nucl. Instr. and Meth. **A350** (1994) 57;
H1 Calorimeter Group, B. Andrieu et al., Nucl. Instr. and Meth. **A336** (1993) 499.

[13] H1 SPACAL Group, R. D. Appuhn et al., Nucl. Instr. and Meth. **A386** (1997) 397.

[14] A. Meyer, PhD thesis, University of Hamburg, 1997, DESY FH1-97-01.

[15] F. Lehner, PhD thesis, University of Hamburg, 1998, DESY-THESIS-1998-003.

[16] H1 Collaboration, Technical Proposal for the Upgrade of the Backward Region of the H1 Detector, DESY internal report PRC-93/02.

[17] H1 Collaboration, C. Adloff et al., Nucl. Phys. **B497** (1997) 3.

[18] J. Chýla, J. Cvach, Proceedings of the International Conference on the Structure and Interactions of the Photon, PHOTON '97, Edmond aan Zee, World Scientific, p. 156.

[19] G. Marchesini et al., Comp. Phys. Commmun. 67 (1992), 1.
(HERWIG version 5.9 was used).

[20] H. Jung, Comp. Phys. Commun. 86 (1995) 147.
(RAPGAP version 2.6 was used).

[21] JETSET 7.3 and 7.4, T. Sjöstrand, Comput. Phys. Com. 82 (1994) 74.

[22] G. Gustafson and U. Petterson, Nucl. Phys. **B306** (1988) 746;
B. Andersson et al., Z. Phys. **C43** (1989) 625.

[23] M. Taševský, PhD thesis, Charles University, Prague, 1999, unpublished.

[24] M. Drees, R. Godbole, Phys. Rev. **D50** (1994) 3124.

[25] G. D'Agostini, Nucl. Instr. and Meth.**A362** (1995) 487.

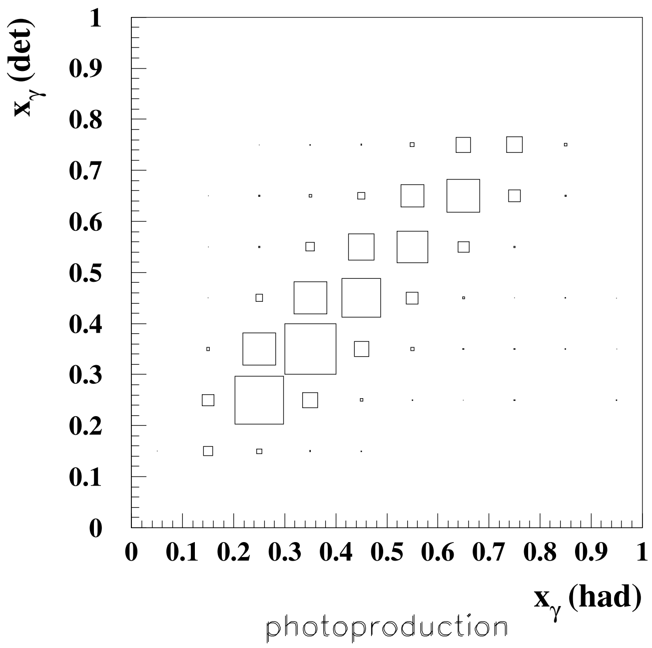

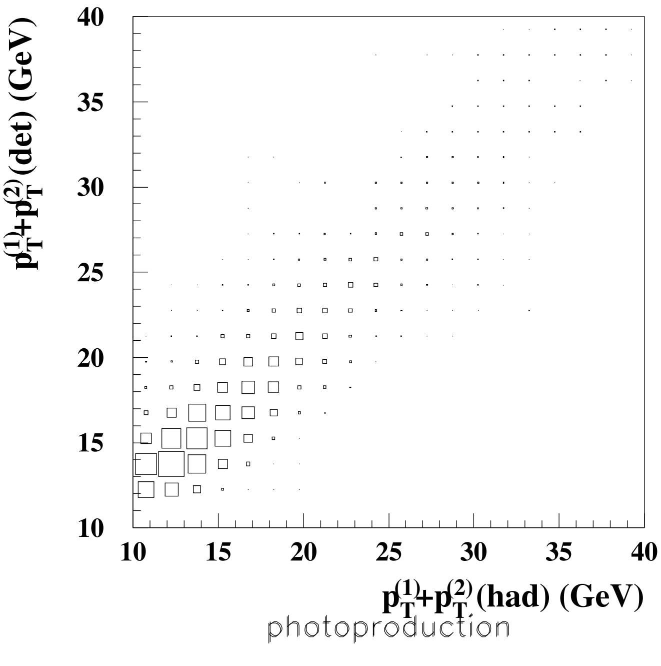

Figure 1: The correlation of x_γ and $p_T^{(1)} + p_T^{(2)}$ of the two hard jets at the hadron and detector level (photoproduction sample of HERWIG).

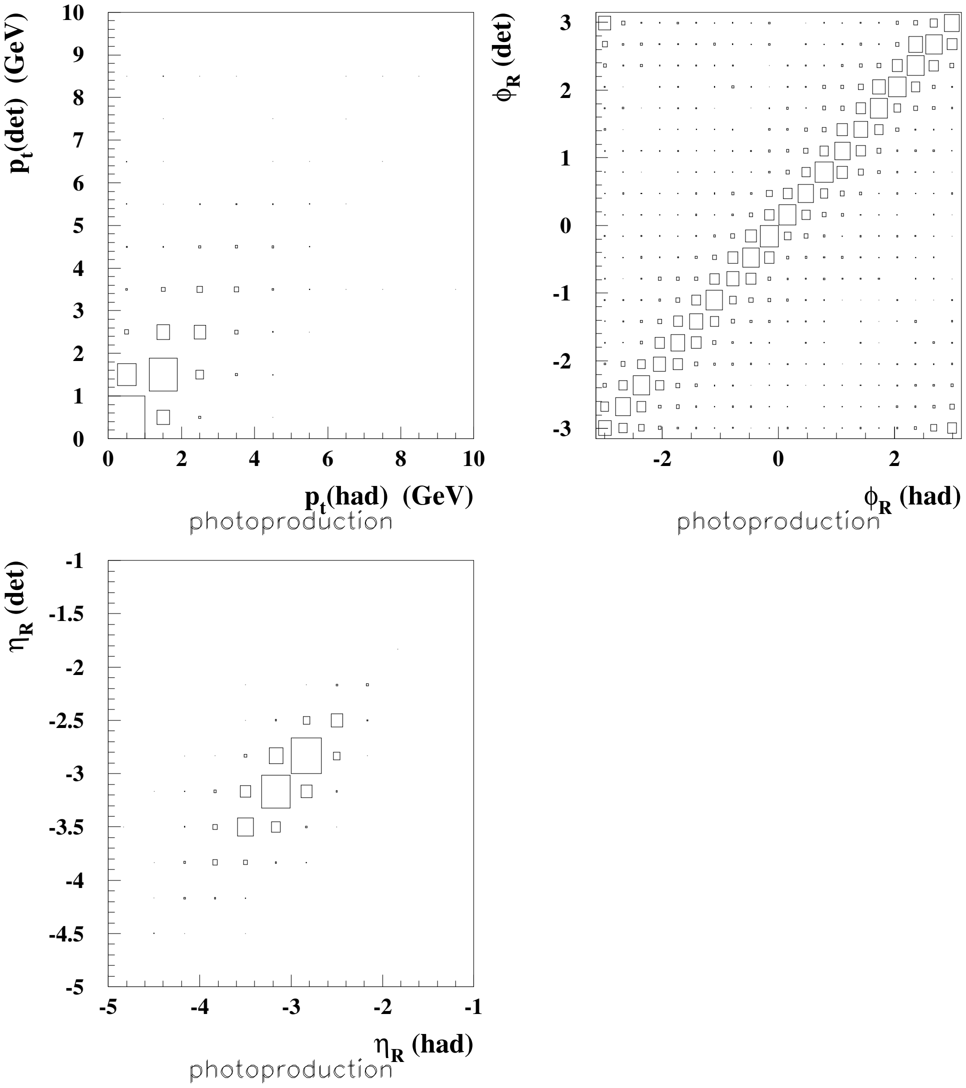

Figure 2: The correlation of p_t ,φ_R and η_R of the photon remnant jet at the hadron and detector level (photoproduction sample of HERWIG).

H1 preliminary

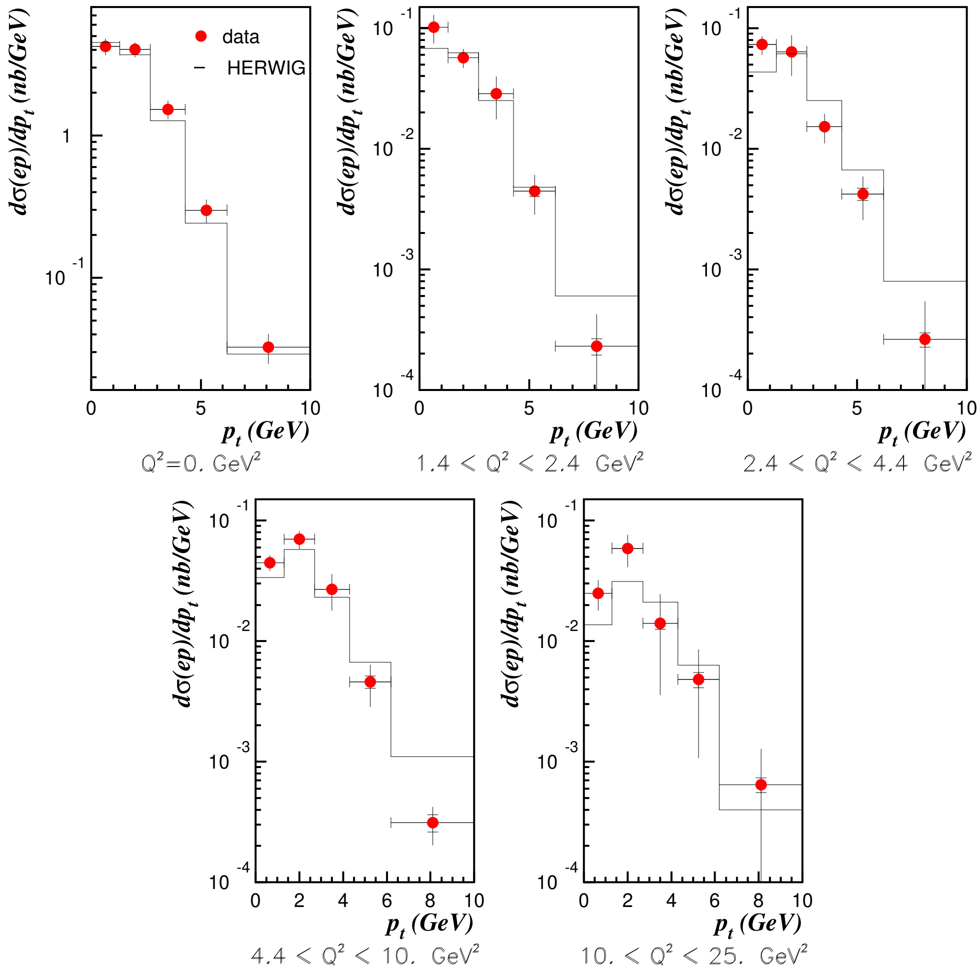

Figure 3: The differential cross section $d\sigma/dp_t$ of the photon remnant jet for the data (points) and HERWIG (histogram) in intervals of the photon virtuality Q^2. (Cut for resolved events: $x_\gamma < 0.75$, hard jet cuts: $p_T^{(i)} > 5$ GeV, $-3. < \eta^{(i)} < 0.$ (i=1,2) and $p_T^{(1)} + p_T^{(2)} > 12$ GeV)

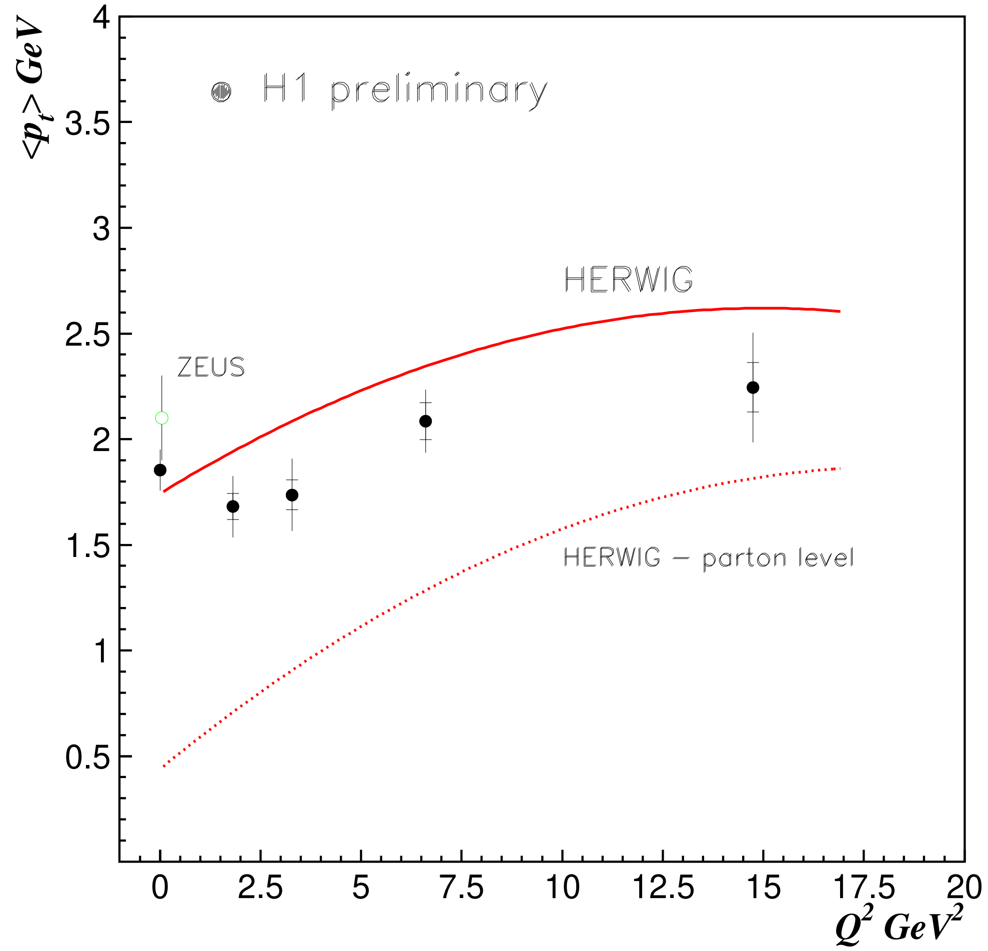

Figure 4: The mean p_t of the photon remnant jet for data (points) and HERWIG (curves) for hadron and parton level, as a function of the photon virtuality Q^2. (Cut for resolved events: $x_\gamma < 0.75$, hard jet cuts: $p_T^{(i)} > 5$ GeV, $-3. < \eta^{(i)} < 0.$ (i=1,2) and $p_T^{(1)} + p_T^{(2)} > 12$ GeV.)

H1 preliminary

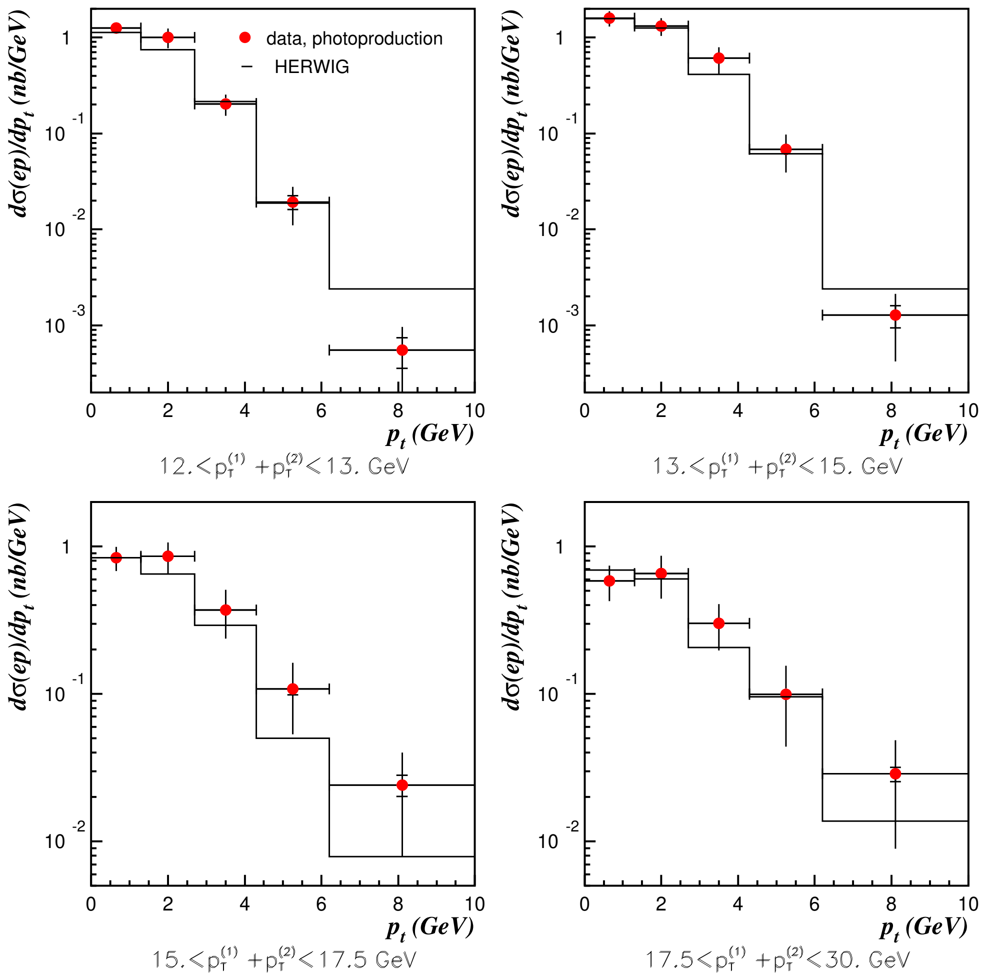

Figure 5: The differential cross section $d\sigma/dp_t$ of the photon remnant jet for the photoproduction data (points) and HERWIG (histogram) in intervals of the hard scale $p_T^{(1)} + p_T^{(2)}$. (Cut for resolved events: $x_\gamma < 0.75$, hard jet cuts: $p_T^{(i)} > 5$ GeV, $-3. < \eta^{(i)} < 0.$ (i=1,2) and $p_T^{(1)} + p_T^{(2)} > 12$ GeV.)

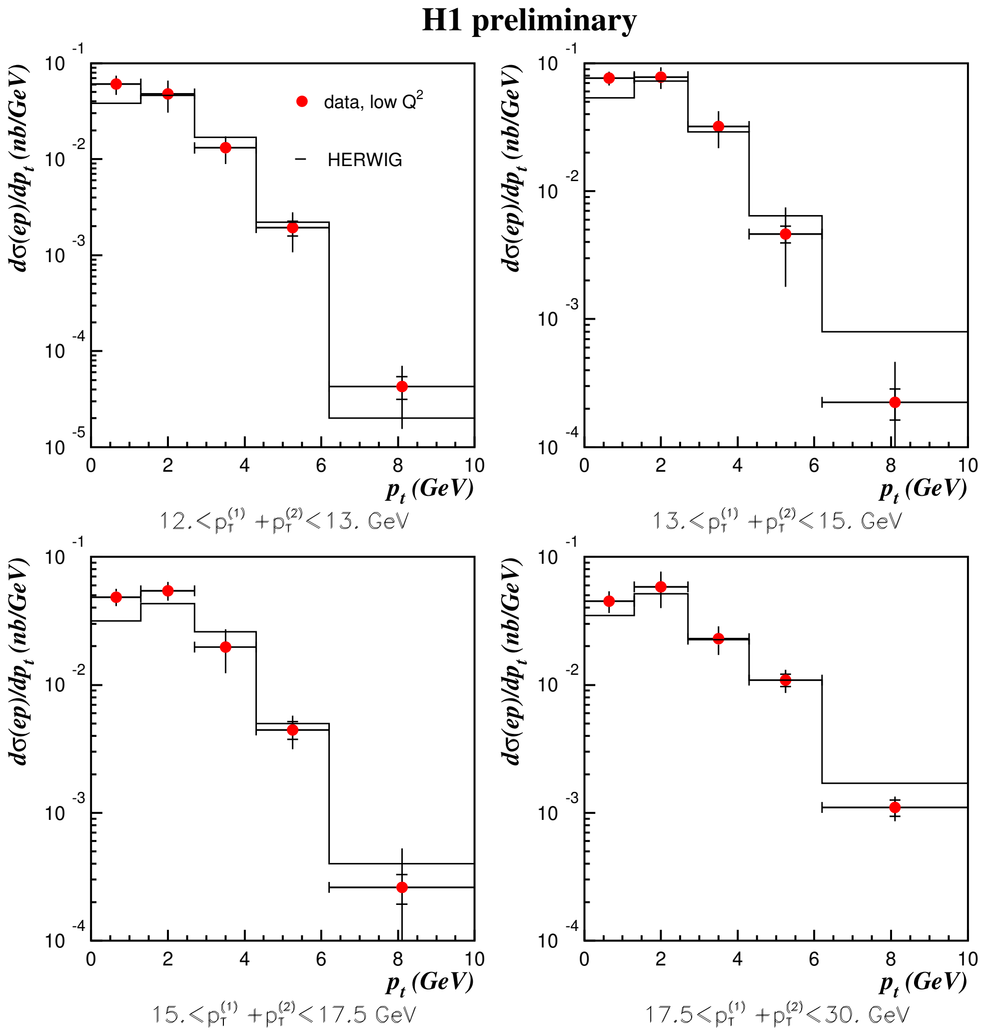

Figure 6: The differential cross section $d\sigma/dp_t$ of the photon remnant jet for low Q^2 data (points) and HERWIG (histogram) in intervals of the hard scale $p_T^{(1)} + p_T^{(2)}$. (Cut for resolved events: $x_\gamma < 0.75$, hard jet cuts: $p_T^{(i)} > 5$ GeV, $-3. < \eta^{(i)} < 0.$ (i=1,2) and $p_T^{(1)} + p_T^{(2)} > 12$ GeV.)

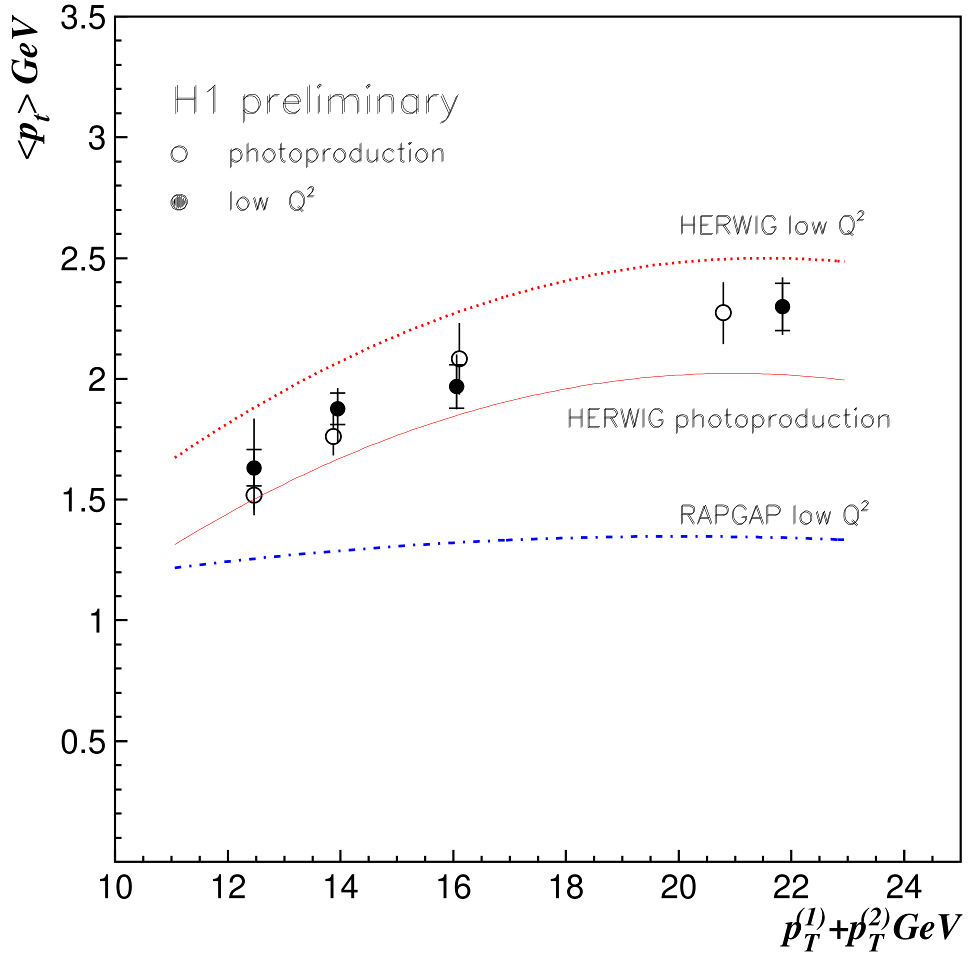

Figure 7: The mean p_t of the photon remnant jet for photoproduction (open circles) and low Q^2 (full circles) data as a function of the hard scale $p_T^{(1)}+p_T^{(2)}$ compared with HERWIG and RAPGAP predictions. (Cut for resolved events: $x_\gamma < 0.75$, hard jet cuts: $p_T^{(i)} > 5$ GeV, $-3. < \eta^{(i)} < 0.$ (i=1,2) and $p_T^{(1)}+p_T^{(2)} >$ 12 GeV.)